Applied Catalysis B: Environmental 191 (2016) 1–7

Contents lists available at ScienceDirect

Applied Catalysis B: Environmental

journal homepage: www.elsevier.com/locate/apcatb

Ni and Ni-Co $La_{0.8}Sr_{0.2}Ga_{0.8}Mg_{0.2}O_{3-\delta}$ infiltrated cells in $H_2$and CH_4/CO_2 mixture

Elisabetta Di Bartolomeo[a,*], Francesco Basoli[a], Igor Luisetto[b], Simonetta Tuti[b], Francesca Zurlo[a], Zahra Salehi[a], Silvia Licoccia[a]

[a] Department of Chemical Science and Technologies, University of Rome Tor Vergata, Via della Ricerca Scientifica, 00133 Rome, Italy
[b] Department of Science, University of Roma Tre, via della Vasca Navale, 00146 Rome, Italy

ARTICLE INFO

Article history:
Received 25 November 2015
Received in revised form 29 February 2016
Accepted 4 March 2016
Available online 10 March 2016

Keywords:
SOFC
Infiltrated anodes
Electrochemical measurements
Dry reforming of methane
Impregnated LSGM powders
Catalytic measurements

ABSTRACT

$La_{0.8}Sr_{0.2}Ga_{0.8}Mg_{0.2}O_{3-\delta}$(LSGM) based fuel cells infiltrated with different metal catalysts were fabricated and tested both in H_2 and CH_4/CO_2mixture. Ni, Co, Ni-Cu, Ni-Co LSGM impregnated powders were investigated for the dry reforming of methane reaction (DRM) ($CH_4 + CO_2 \leftrightarrows 2CO + 2H_2$). The catalytic activity for CH_4 and CO_2 conversion followed the order Ni∼Ni-Co > Co > Ni-Cu. Both Ni and Ni-Co catalysts, investigated versus time (50 h) on stream of CH_4/CO_2 = 1.5 at 800 °C, did not show any sign of deactivation indicating their stability toward coke deposition. Anyway, evidence of few carbon filaments was revealed by SEM micrographs and the carbon amount evaluated by TG-DTA analysis. Ni-LSGM and Ni-CoLSGM cells showed regarding electrochemical performance both in H_2 and CH_4/CO_2 mixture in the 650–750 °C temperature range. A discussion on the parallelism between catalytic and electrochemical performance is detailed.

1. Introduction

Solid oxide fuel cells (SOFCs) are considered among the most promising resources for distributed power applications because of their fuel flexibility. However, long lasting systems that can operate on a range of fuels are not yet available and are still subject to intense research and development [1]. Most commonly used Ni/YSZ anodes are highly optimized for H_2 and syn gas (H_2 and CO) but are not stable when exposed to hydrocarbons (due to carbon formation) moreover show very low tolerance to hydrogen sulfide (H_2S) always present as impurity especially in biofuels.

Biogas containing CO_2 can be reformed directly into SOFC stacks. For this purpose it is necessary to develop catalytic materials which meet the constraints dictated by the anodic properties, i.e. the ionic and electronic conductivity.

The application of the DRM for syn-gas production has been widely studied [2–6]. Catalysts that are more resistant toward-coking are those based on Ni nanoparticles highly dispersed over oxides with strong surface basicity [7–10]. Their properties are not functional for the implementation in the anodes due to the low Ni content (<10 wt%) and the nature of the oxide carrier. In order to decrease the carbon formation tendency of Ni the use of bimetallic system containing Co and Cu has been proven to be an efficient strategy due to the formation of alloys that are inherently more stable apart from particle size dimension [11–13].

In recent years many efforts have been devoted to improve performance and stability mainly addressing microstructural control. The strategies to overcome the limitations of the conventional anodic cermet can be summarized as in the following: enhancing the performance of Ni/YSZ anodes i.e., adding a second catalyst to reduce carbon formation [14,15] or applying a thin protecting layer [16], using metals alternative to Ni for electronic conduction i.e. infiltrating Cu, Ni, Co, Fe [17–19] or oxide components [20–22] into porous YSZ scaffolds, or using ceramic anodes mainly with perovskite structure that provide electronic conduction in reducing conditions [23–29].

To obtain cells performing at reduced operating temperatures (≤750 °C), $La_{0.8}Sr_{0.2}Ga_{0.8}Mg_{0.2}O_{3-\delta}$ (LSGM) is a promising electrolyte for its high ionic conductivity and negligible electronic contribution over a wide partial pressure range [30,31]. The main drawback of LSGM is its chemical reactivity with Ni during the co-firing process which produces undesired insulating phases (above 1100 °C) [32]. Thus, a two steps procedure has been tuned: a high temperature step (1450 °C) for the porous/dense bilayer fabrication and a lower temperature step (700 °C) for the infiltration. Moreover, the infiltration produces a nano-porous metal coating on the

* Corresponding author.
E-mail address: dibartolomeo@uniroma2.it (E. Di Bartolomeo).

http://dx.doi.org/10.1016/j.apcatb.2016.03.010
0926-3373/

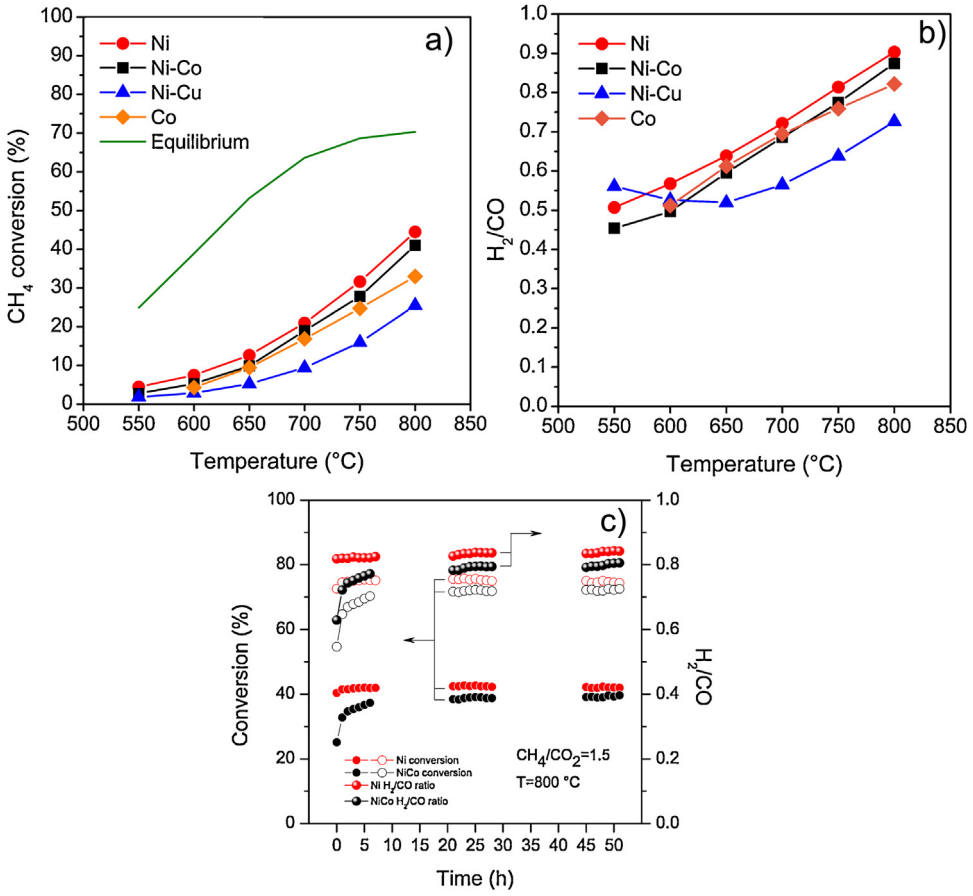

Fig. 1. Catalytic activity for the DMR reaction of different metal catalysts impregnated LSGM powder: CH_4 conversion as a function of temperature (a), selectivity versus temperature (b), and CH_4 (closed symbols) and CO_2 (open symbols) conversions versus time of Ni and Ni-Co impregnated catalysts at 800 °C (c). Reaction conditions CH_4/CO_2 = 1.5 and GHSV = 120000 ml g^{-1} h^{-1}.

surface of porous anodic scaffold that can improve the triple phase boundary (TPB) density, reducing the anodic polarization resistance [33,34].

In the present work, LSGM based fuel cells were infiltrated with different metal catalysts and measured both in H_2 and CH_4:CO_2 = 60:40 vol% mixture (typical biogas composition). Ni, Co, Ni-Cu, Ni-Co LSGM impregnated powders with the same amount of catalyst of the infiltrated cells and necessary to behave as a performing anode were investigated for the dry reforming of methane reaction (DRM) ($CH_4 + CO_2 \leftrightarrows 2CO + 2H_2$). The catalytic activity for CH_4 and CO_2 conversion followed the order Ni∼Ni-Co > Co > Ni-Cu. Ni and Ni-Co infiltrated cells showed good performance both in H_2 and in CH_4/CO_2 exposure in comparison to relevant literature [1,4–8,21,22]. The body of results supplies a parallelism between the catalytic measurements on LSGM impregnated powders and the electrochemical performance of infiltrated cells in CH_4/CO_2 mixture.

2. Experimental

2.1. Catalyst preparation

Catalysts with 25 wt% of metals content were prepared by wet impregnation method: aqueous metals (Ni, Co and Cu) nitrates salt solutions were added to a commercial LSGM powder to form a slurry. The solvent was evaporated at 60 °C under vigorous stirring. The impregnated LSGM was further dried at 100 °C overnight and calcined at 700 °C for 1 h.

2.2. Catalytic activity

The catalytic activity was measured in a fixed-bed quartz reactor at atmospheric pressure connected to a flow apparatus equipped with mass flow controllers. The dry reforming of methane was studied with a mixture of CH_4:CO_2:Ar = 48:32:20 vol% and a total flow rate of 100 $cm^3 min^{-1}$ (GHSW 120,000 cm^3 g^{-1} h^{-1}). Catalysts (0.050 g) were reduced in-situ with 50% H_2/Ar flow (30 cm^3 min^{-1}) increasing the reactor temperature from RT up to 800 °C with a ramp of about 10 °Cmin^{-1} and isothermally kept at this temperature for 1 h. Then, the gas flow was switched to the reactant mixture and the catalytic run was performed in the temperature ranged 550–800 °C.Gas composition was analyzed by Agilent 7820 gas-chromatograph equipped with Molecular sieve X13 (for the H_2, Ar, CO, CH_4 separation), Hayesep Q (for CO_2 separation) columns and a TCD detector.

CH_4 and CO_2 percent conversions (X_i %) were calculated according to Eq. (1) using Ar as internal standard.

$$X_i(\%) = 100 \times \left(1 - \frac{C_i \cdot C^0_{Ar}}{C^0_i \cdot C_{Ar}}\right) \quad (1)$$

where C^0_i and C^0_{Ar} are the inlet concentrations of the reactants (i = CH_4 or CO_2) and Ar respectively and C_i and C_{Ar} are the corresponding outlet concentrations. Thermodinamic equilibrium conversions were calculated using GASEQ software.

To evaluate the amount of deposited carbon after time on stream measurements, simultaneous termogravimetric (TG) and differential thermal analysis (DTA) was performed on Ni and Ni-Co LSGM impregnated powders by using TG-DSC 1 (Mettler Toledo, STAR

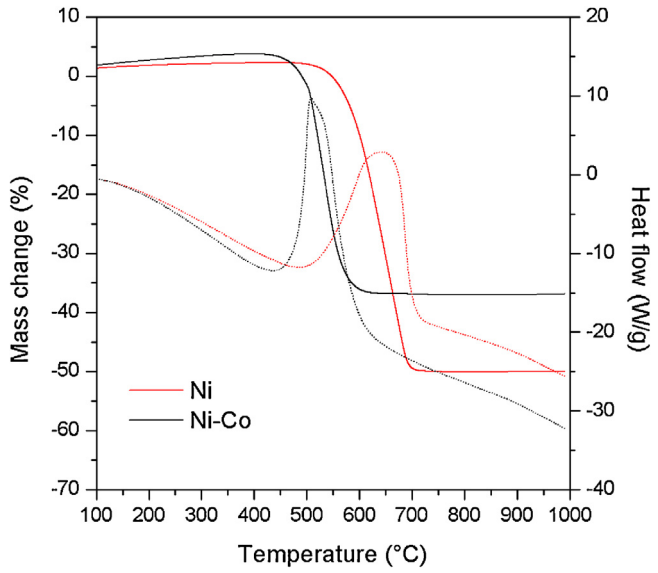

Fig. 2. TG (solid line)DTA (dotted line) analysis of Ni (red) and Ni-Co (black) impregnated catalysts. (For interpretation of the references to colour in this figure legend, the reader is referred to the web version of this article.)

System). The samples (~15 mg) were loaded in a Pt crucible and oxidized (50 cm^3 min^{-1}) to 1000 °C at 5 °C min^{-1}.

2.3. Porous/dense bilayer

LSGM commercial powders purchased by Praxair (0.8 m^2 g^{-1}) were used for the fabrication of both anode and spun electrolyte layers. Supporting anodes were prepared by die pressing method: LSGM (45 wt%), BUTVAR98 (Sigma Aldrich) (5 wt%), pore formers (55 wt%) were planetary ball milled at 250 rounds per minutes (RPM) for 30 min using hexane as solvent. The pore formers were 15 wt% of micrometric carbon (Sigma Aldrich) and 40 wt% of micrometric spheres of PMMA (AltuglassBS150N) giving an open porosity of 66% effective for the infiltration procedure [35]. The slurry was dried at 60 °C overnight, then the powder was grounded in an agate mortar and uniaxially pressed at 100 MPa into cylindrical pellets of 13 mm in diameter. The porous pellets were pre-sintered at 1250 °C for 6 h with heating rate of 5 °C min^{-1} to get a proper mechanical strength to be used as substrate for the spin coating. The spin coating technique was chosen because particularly useful for lab scale application since it allows the use of small amounts of materials. Dense LSGM membranes were fabricated by spinning a suspension of LSGM(25 wt%) in a mixture of organic solvents (terpineol:ethanol 1:1vol%) with BUTVAR98 as binder (5 wt%), polyethyleneglycol PEG400(3 wt%) and di-*n* butyl phathalate DBP (3 wt%) as plasticizers. The slurry was spin coated on the pre-sintered anodes then dried at 80 °C for 30 min and thermally treated at 400 °C for 1 h to remove the organics. To reach the desired electrolyte thickness, the spin coating process was repeated and a strict control of the final film thickness was obtained [36]; finally, the half cell was co-sintered at 1450 °C for 6 h.

$La_{0.6}Sr_{0.4}Fe_{0.8}Co_{0.2}O_{3-\delta}$ (LSCF) commercial powder (Praxair) was employed as cathode, manually deposited on the electrolyte and calcined at 900 °C for 2 h. Gold paste and wires were used as current collectors both for the anode and cathode side and fired at 700 °C for 30 min.

Structural and morphological characterizations of powders, pellets and half cells were performed by X-ray diffraction (XRD) analysis (Philips X-Pert Pro 500 Diffractometer) and Field Emission Scanning Electron Microscopy (SUPRA^{TM} 35, Carl Zeiss SMT, Oberkochen, Germany).

2.4. Infiltration

To introduce the catalytic component into the anodic substrates, the LSGM porous scaffolds were infiltrated by a 4 M aqueous solution of either Ni nitrate or Co nitrate (purity 99% by Aldrich) or their 1:1 molar mixture. The infiltrated samples were dried at 400 °C for 1 h and finally calcined at 700 °C for 30 min. Multiple impregnation/calcinations cycles were necessary to introduce a proper amount of metal catalyst into the LSGM scaffolds. Finally, metal oxide was reduced upon hydrogen exposure at high temperature (up to 750 °C) during the cell heating.

2.5. Cell tests

For fuel cell tests, the single cells were mounted at the end of an alumina tube using a gas tight ceramic paste seal (Aremco,552). Fuel-air fuel cell experiments were carried out between 650 and 750 °C. The cathode was exposed to static air while the anode to H_2 or CH_4:CO_2 = 60:40 mixture (60vol% of CH_4 and 40vol% of CO_2 is the typical composition of biogas) and the total gas flow was maintained at 100 $cm^3 \cdot min^{-1}$. Electrochemical tests were performed using a potentiostat/galvanostat/FRAPARSTAT 2273. Electrochemical impedance spectroscopy (EIS) measurements were carried out between 600 and 750 °C in the frequency range between 0.2 Hz and 2 MHz with AC voltage amplitude of 100 mV under open circuit voltage (OCV). Structural and morphological characterizations of the cells were performed both before and after fuel cell tests.

3. Results and discussion

3.1. Catalytic activity of impregnated LSGM powders

Ex-situ catalyst activity measurements for the dry reforming of methane (Eq. (2)) were performed for an initial catalyst screening

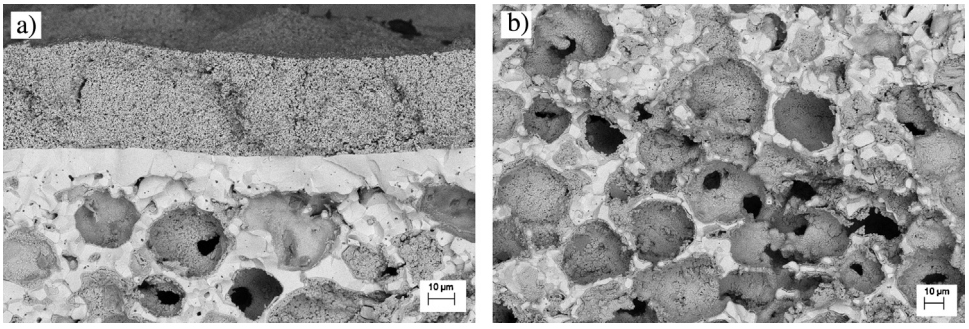

Fig. 3. SEM micrographs (backscattered detector) of cross section of: (a) Ni infiltrated cell and (b) infiltrated scaffold..

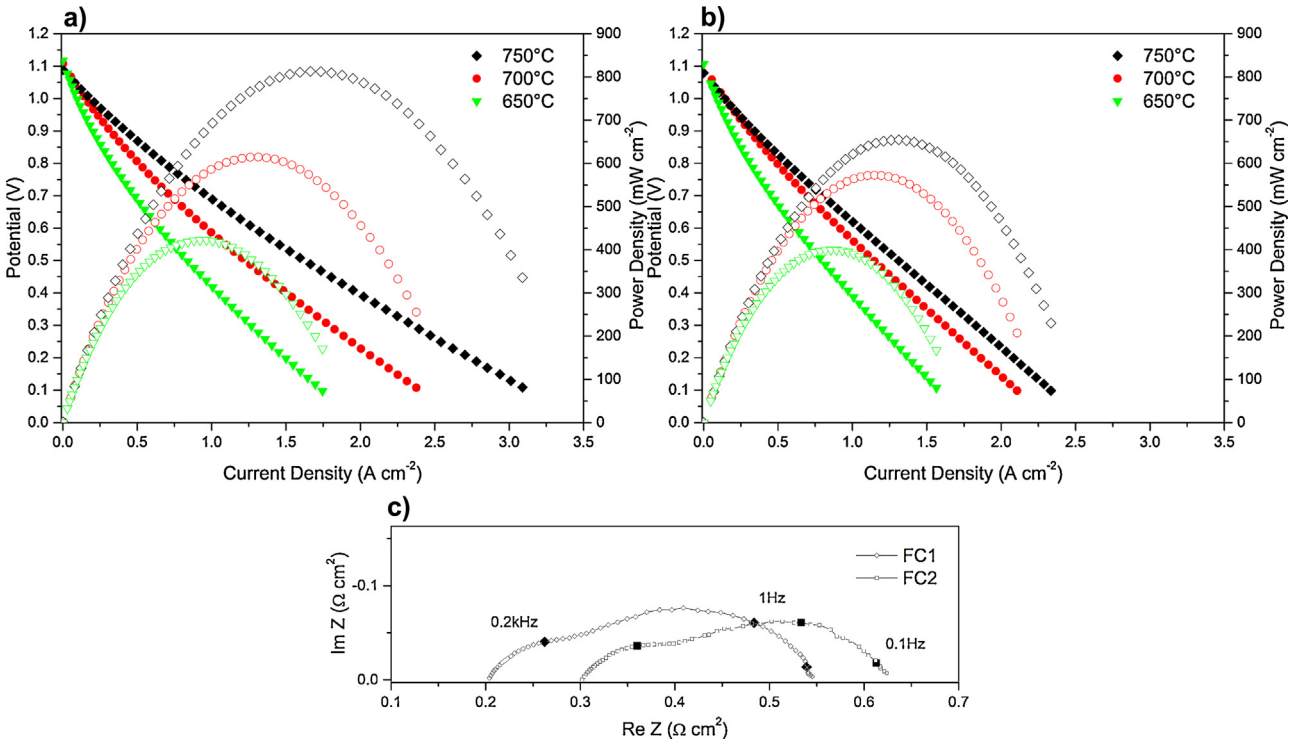

Fig. 4. I–V and power density curves of FC1 (a), FC2 (b) in H_2 between 650 and 750 °C and Nyquist plots at OCV of FC1 and FC2 in H_2 at 750 °C (c).

at an high GHSV to obtain conversions values far from equilibrium to better highlight the differences between catalysts.

$$CH_4+CO_2 \rightleftharpoons 2H_2+2CO \qquad \Delta H^0_{298K} = 247 kJmol^{-1} \qquad (2)$$

Fig. 1 shows the catalytic activity for the DMR reaction of different metal catalysts impregnated LSGM powder: CH_4 conversion as a function of temperature (a), selectivity versus temperature (b), and CH_4 and CO_2 conversions versus time of Ni and Ni-Co impregnated catalyst at 800 °C (c), respectively. Reaction conditions were: $CH_4/CO_2 = 1.5$ and GHSV = 120000 ml g^{-1} h^{-1}. Being the DRM reaction thermodynamically and kinetically favored at high temperatures, the conversions increased in the 550–800 °C temperature range. The CO_2 conversions were larger than that of methane at all temperatures, indicating the occurrence of the side reverse water gas shift reaction (Eq. 3)

$$H_2+CO_2 \rightleftharpoons CO+H_2O \qquad \Delta H^0_{298K} = 41 kJmol^{-1} \qquad (3)$$

The catalytic activity for CH_4 and CO_2 conversion followed the order Ni∼Ni-Co > Co > Ni-Cu. CH_4 dehydrogenation over metallic sites has been recognized as the rate determining step for the DRM reaction [37,38], therefore the observed trend is related to the ability of the different metallic nanoparticles to activate the C—H bond. In particular, Ni was by far the most active transition metal, while Cu strongly decreased the reforming activity. Co is known to show low catalytic activity and low affinity toward carbon and to decrease the metal particle size in metallic alloys reducing the overall carbon affinity [39–42]. Data in Fig. 1a shows that the addition of Co to Ni only slightly decreased the catalytic activity, thus Ni-Co alloys may couple the high catalytic activity of Ni with the high sintering resistance and low carbon affinity of Co yielding to a greatly performing catalysts. The selectivity of different catalysts for the dry reforming reaction, expressed as H_2/CO ratio and reported in Fig. 1b, increased with temperature reaching values of ∼ 0.9, close to the thermodynamic value, both for Ni and Ni-Co catalysts. The measured carbon balance was close 100% for both catalysts indicating that the decompositon of CH_4 is less favored than DMR reaction. Differences in H_2/CO ratio for the catalysts reflected the differences in the catalytic activity and the lower reactants conversion yields a lower H_2/CO ratio. In fact the RWGS, which is responsible for the low H_2/CO ratio, is reported to be near equilibrium in the measured temperature range [25,26]. Increasing the temperature the CO_2 is coverted in the DMR and its small amount available for RWGS gives a H_2/CO_2 ratio close to unit.

In the DRM reaction, the reactive carbon atoms (C*) formed by dehydrogenation of methane on the metallic surface are oxidized to CO; however, if the rate of C* oxidation is lower than that of CH_4 dehydrogenation, C* accumulate and may be converted to less reactive carbon species, which encapsulate the surface of metallic site or form carbon filaments, leading to a rapid catalyst deactivation due to reactant blockage. To assess the stability toward coke deposition, Ni and Ni-Co catalysts were investigated versus time on stream of $CH_4/CO_2 = 1.5$ at 800 °C as reported in Fig. 1c. Both methane and carbon dioxide conversions were stable without any sign of deactivation during 50 h, indicating good stability of both impregnated powders in conditions ($CH_4/CO_2 = 1.5$) where the carbon formation is highly favored. Anyway, from SEM investigation reported in *Supplementary material* section (Fig. S1) the presence of carbon filaments was revealed for both Ni and Ni-Co impregnated powders. The amount of carbon deposited during 50 h on stream was evaluated by TG-DTA analysis and shown in Fig. 2. The total amount of deposited carbon was about 36% and 50% of the initial weight for Ni-Co and Ni catalysts, respectively. From the heat flow curves an exothermic peak is clearly visible around 500° and 650 °C for Ni-Co and Ni LSGM powders, respectively; thus the carbon deposited on Ni-Co impregnated powders is more easily oxidizable at lower temperature. Even though a large amount of carbon was deposited on both infiltrated powders, the catalysts were not deactivated over 50 h of stream in unfavoured conditions and the carbon deposited on Ni-Co LSGM is completely oxidized below 600 °C that can be a key point for the removal of carbon deposits on the anode operating in IT range. In fact, the oxygen ions coming from the cathode side through the electrolyte to the inter-

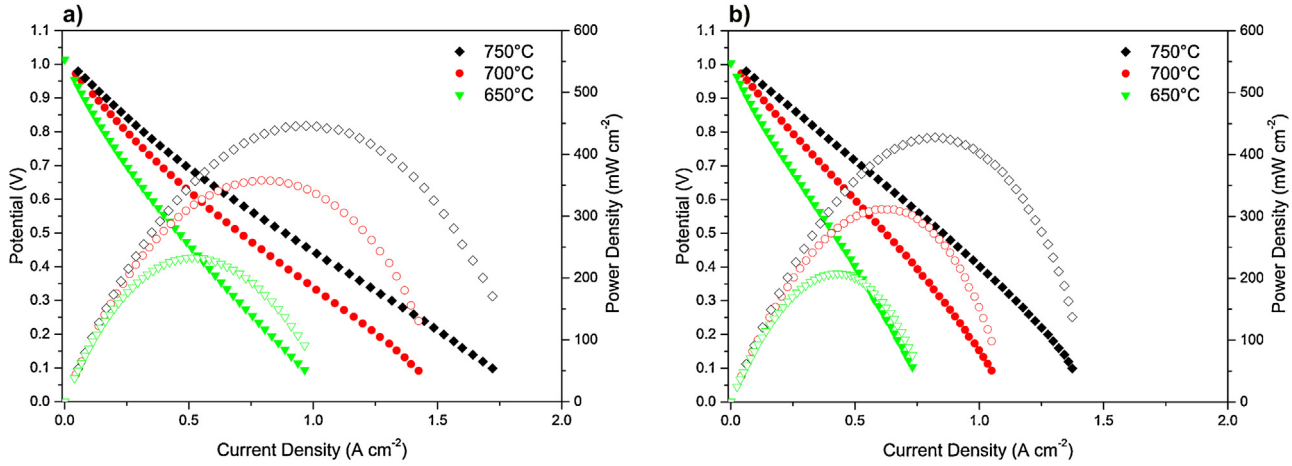

Fig. 5. I–V and power density curves of FC1 (a) and FC2 (b) in 100 cm^3 min^{-1} of CH_4:CO_2 = 60:40 between 650 and 750 °C.

Table 1
Performance of FC1 and FC2 operating in CH_4/CO_2 mixture at various temperatures.

	FC1			FC2		
Temperature (°C)	650	700	750	650	700	750
OCV (V)	1.01	1.01	1.02	1.00	1.01	1.02
P ($mWcm^{-2}$)	233	358	446	208	312	428
R_{ohm} (ohm cm^2)	0.56	0.41	0.36	0.48	0.39	0.35
R_{pol} (ohm cm^2)	0.89	0.46	0.33	0.98	0.55	0.36
R_{tot}(ohm cm^2)	1.45	0.87	0.69	1.46	0.94	0.71

face anode/electrolyte can oxidize the deposited carbon, especially at high current desities, contributing to the CO/CO_2 formation in a relatively low temperature range thus improving the overall coking resistance.

3.2. Cell fabrication

Porous anodic substrates (66% of porosity) with a fully dense micrometric LSGM membrane were obtained after a co-sintering at 1450 °C for 6 h. An amount of ~25 wt% of Ni, Co metals and Ni-Co alloy was infiltrated into the scaffold. Fig. 3a and b shows the SEM micrographs of the cross section of a Ni infiltrated cell. The electrolyte was about 13–15 μm thick and fully dense, the cathode (30–40 μm thick) was porous and properly attached to the electrolyte surface. The infiltrated anodic scaffold (Fig. 3b) showed micrometric open pores with a continuous nano-porous Ni coating.To check the chemical stability and the possible formation of new phases, XRD analysis of infiltrated half cells were performed after drying at 400 °C and calcination at 700 °C. Data are reported in *Supplementary material*section (Figs. S2 and S3). Before infiltration, the half cells showed the same XRD pattern (JCPS 88-0061) of the starting powders, only slightly shifted (<0.5°) toward higher angles probably because of a misalignment of the bulky sample (data not shown). After drying at 400 °C, the XRD pattern (Fig. S2) showed the peaks of perovskite phase and NiO phases, in accordance with previously reported data [32]. After firing at 700 °C, the LSGM structure was preserved and the NiO peaks were clearly detected (JCPS 71-1179). Moreover, SrO (JCPS 74-1227) secondary phase was observed, indicating that some cations interdiffusion was taking place at 700 °C. In the Ni-Co infiltrated cell, quite broad peaks ascribable to NiO and Co_3O_4 (JCPS 42-1467) phases were observed after drying at 400 °C (Fig. S3). After calcinations at 700 °C, NiO and Co_3O_4 were clearly detectable together with some peaks of LSGM. In both XRD patterns, some minor peaks, hardly distinguishable from the baseline and corresponding to a few percent of unknown secondary phases are present even if not affecting the conductivity of the sample. Thus, the infiltration process and the subsequent heating treatment preserve the phase components.

3.3. Electrochemical performance

Cell tests were performed on cells infiltrated with the same amount, 25 wt.%, of Ni and Ni-Co catalysts both in H_2 and CH_4:CO_2 = 60:40. The Ni infiltrated cell is labeled FC1 and Ni-Co infiltrated cell FC2.

Microstructural analysis showed that in FC1 the electrolyte was 13–15 μm thick, the cathode was about 40 μm and the anodic substrate was 630–650 μm; in FC2 the electrolyte and the cathode were slightly thicker than in FC1, i.e. the electrolyte was 17–19 μm, the cathode was about 70 μm, and the substrate was 630 μm, the same thickness of FC1.

Fig. 4a and b shows the electrochemical performance of FC1 and FC2 in 100 cm^3 min^{-1} of H_2 in the temperature range between 650 and 750 °C and (c) the Nyquist plots at OCV of FC1 and FC2 in H_2 at 750 °C. The maximum power output of FC1 at 750 °C was 815 mW cm^{-2} and the maximum current density 3.09 A cm^{-2}, whereas, for FC2, the maximum power output at 750 °C was 657 mW cm^{-2} and the maximum current density 2.33 A cm^{-2}. FC1 showed better performance than FC2 especially at the highest temperature (750 °C) and the maximum power output values of both cells were decreasing by reducing the operating temperature. The OCV values of FC1 were slightly larger (1.10 V at 750 °C) than that of FC2 (1.05 V) probably due to some microstructural defects in the sealing materials of cell assembly.

To get a deeper insight on the observed differences in the electrochemical performance, EIS spectra at OCV were recorded. The high frequency real axis intercept is the ohmic resistance (R_{ohm}) which is contributed mainly by the electrolyte, whereas the difference between the low and high frequency real axis intercepts is the electrodes polarization resistance (R_{pol}). R_{ohm} of FC1 was lower than FC2 (0.20 ohm cm^2 compared with 0.30 ohm cm^2) as it was expected being the FC1 electrolyte slightly thinner (13–15 μm instead of 17–19 μm) whereas R_{pol} values were very similar (0.30 ohm cm^2). Deconvoluting the polarization contributions, at least two semicircles (at low and high frequency) were revealed that can be ascribed to the anodic and cathodic contributions. To further evaluate the polarization characteristics of the cells, I–V and power density curves and EIS measurements of FC1 at 750 °C at two different hydrogen concentrations (100% H_2 and 20%H_2 in Ar) were performed. Data are reported in Supplementary material Section (Fig. S4). Depleting the fuel at the anodic interface, both the OCV and the current density values (especially at low volt-

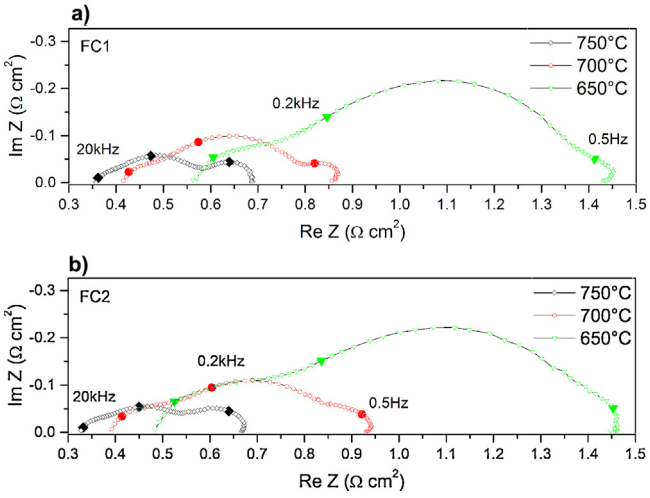

Fig. 6. Nyquist plots at OCV of FC1 (a) and FC2 (b) in 100 cm^3 min^{-1} of CH_4:CO_2 = 60:40 between 650 and 750 °C.

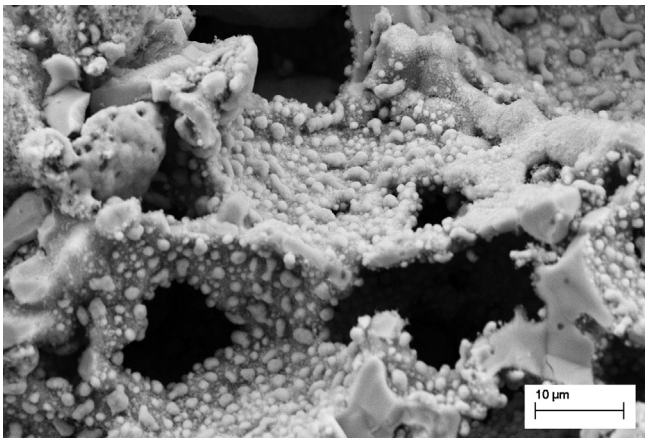

Fig. 7. SEM micrographs of Ni/Co infiltrated anode after cell tests measurements.

ages) decreased. In the EIS spectra, the low frequency semicircle, most likely related to a mass transport effect, increased, identifying the low frequency contribution as ascribable to the anode while the high frequency semicircle, being constant, was referred to the cathode contribution. The constant cathodic contribution proved a negligible cation interdiffusion at LSFC/LSGM interface ensuring a good stability of the cell [27]. At reduced hydrogen partial pressure, R_{ohm} slightly increased, probably, because of a local reduction of temperature due to a reduced H_2 oxidation.

FC1 and FC2 were also tested in CH_4:CO_2 = 60:40 mixture in a total gas flow of 100 cm^3 min^{-1} as reported in Fig. 5a and b. The performance of Ni and Ni-Co infiltrated cells were quite similar, in agreement with the features of the catalytic measurements performed on the corresponding Ni and Ni-Co (25 wt%) supported on LSGM powders. Likewise to the catalytic screening, the addition of Co to Ni did not reduce the catalytic activity and thus consequently the electrochemical performance of the infiltrated cells. Fig. 6 shows the Nyquist plots at OCV of FC1 (a) and FC2 (b) in 100 cm^3 min^{-1} of CH_4:CO_2 = 60:40 between 650 and 750 °C. The R_{ohm} and R_{pol} values for FC1 and FC2 were very close and three semicircles were deconvoluted from the analysis of the polarization resistance, one more (at lower frequencies) than in the case of H_2 feeding, probably due to the slow mass diffusion of methane in the infiltrated anode. Table 1 summarizes the performance of FC1 and FC2 in CH_4/CO_2. The OCV values of two cells were similar and slightly increasing by increasing temperature most probably due to the less temperature dependence of the standard Nernst potential E° for methane and carbon monoxide oxidation in comparison to E° for hydrogen oxidation [14].

At 750 °C the maximum power output of FC1 and FC2 at 750 °C were 446 mW cm^{-2} and 428 mW cm^{-2}, respectively. From impedance measurements at OCV, the R_{ohm} values of FC1 were slightly larger than that measured in H_2 (Fig. 6) at all investigated temperatures. These features may have two possible explanations: the endothermic nature of the DMR reaction that locally decreases the operating temperature causing an increase in R_{ohm} or the Ni interdiffusion into the electrolyte that reduce the ionic conductivity. Increased R_{ohm} was specifically observed in the Ni infiltrated cell (FC1), i.e. in the presence of the catalytically more active species, while the same R_{ohm} values both in H_2 and CH_4/CO_2 mixture were measured in FC2.The R_{pol} values of FC1 were lower than those of FC2 at all investigated temperatures, confirming the Ni as the most active transition metal toward reforming activity in agreement with the catalytic screening on impregnated powders. Thus, the total resistance values (R_{tot}) of FC1 and FC2 cells were very close giving rise to comparable power output values and similar overall performance in CH_4/CO_2 mixture. Reducing the total flux of CH_4/CO_2 mixture from 100 to 50 cm^3 min^{-1}, the electrochemical performance reported in Supplementary material Section (Fig. S5) shows that the maximum power outputs and the current densities slightly increased indicating that the catalytic conversion of reactant increased, being the contact time enhanced. R_{pol} decreased being reduced the low frequency semicircles attributed to the oxidation and mass diffusion of methane in the anode substrate.

Finally, to investigate carbon formation, an accurate microstructural analysis was performed after cell tests measurements. The fuel cell tests were repeated for 4 subsequent days exactly in the same experimental conditions of Figs. 4 and 5. After 4 days a sealing problem occurred. Thus, the overall exposure of the anode to CH_4/CO_2 mixture was shorter (no more than 20 h) than that of powdered catalysts (50 h reported in Fig. 1c). From the micrograph reported in Fig. 7, no clear evidence of carbon deposition was observed in the anode substrate and EDX (Energy Dispersive X-ray) mapping did not revealed any presence of carbon, while, agglomerations and/or coarsening of metallic catalyst are visible on the LSGM porous structure that can be responsible of the observed polarization resistance increase. The lack of carbon filaments can be explained by the re-oxidation of few deposited carbon due to the oxygen coming from the cathode side, thus, showing the anode a good overall coking resistance.

Further work will be devoted to assess the coking-resistance of the anodes by a systematic comparison of the long-term stability measurements of catalysts and single cells.

4. Conclusions

The catalytic investigation of 25 wt% metal catalyst impregnated LSGM powders showed that the addition of Co to Ni only slightly decreased the catalytic activity toward DMR reaction promoting good stability, lower carbon deposition and carbon oxidation at lower temperature (500 °C).

The electrochemical performance of Ni and Ni-Co LSGM infiltrated cells showed promising and comparable performance in CH_4/CO_2 mixture, in agreement with the results of the catalytic investigation. After cell test measurements no evidence of carbon deposition was detected. When a real biogas is fed at the anode side, the main problem is the degradation due not only to carbon coking but also to sulfur poisoning, thus, further work is foreseen to carefully address the durability of LSGM infiltrated cells.

Acknowledgements

The authors gratefully acknowledge the financial support of the Italian Ministry for Education, University and Research (PRIN-2010-2011-Prot.2010KHLKFC).

Appendix A. Supplementary data

Supplementary data associated with this article can be found, in the online version, at http://dx.doi.org/10.1016/j.apcatb.2016.03.010.

References

[1] R. Gorte, J. Vohs, Nanostructured anodes for solid oxide fuel cells, Current Opinion in Colloid & Interface Science 14 (4) (2009) 236–244.
[2] V.C.H. Kroll, H.M. Swaan, C. Mirodatos, Methane reforming reaction with carbon dioxide over Ni/SiO2Catalyst: I. Deactivation studies, J. Catal. 161 (1) (1996) 409–422.
[3] M.C.J. Bradford, M.A. Vannice, CO2 reforming of CH4over supported Pt catalysts, J. Catal. 173 (1) (1998) 157–171.
[4] M.C.J. Bradford, M.A. Vannice, CO2Reforming of CH4, Catal. Rev. 41 (1) (1999) 1–42.
[5] J.-H. Kim, et al., Effect of metal particle size on coking during CO2 reforming of CH4 over Ni–alumina aerogel catalysts, Appl. Cata. A: Gen. 197 (2) (2000) 191–200.
[6] D. Kim, et al., Mechanistic study of the unusual catalytic properties of a new NiCe mixed oxide for the CO2 reforming of methane, J. Catal. 247 (1) (2007) 101–111.
[7] M. Yu, et al., Carbon dioxide reforming of methane over promoted NixMg1-xO (111) platelet catalyst derived from solvothermal synthesis, Appl. Catal. B: Environ. 148–149 (2014) 177–190.
[8] M. Rezaei, et al., CO2 reforming of CH4 over nanocrystalline zirconia-supported nickel catalysts, Appl. Catal. B: Environ. 77 (3–4) (2008) 346–354.
[9] I. Luisetto, et al., Ni/CeO2–Al2O3 catalysts for the dry reforming of methane: the effect of CeAlO3 content and nickel crystallite size on catalytic activity and coke resistance, Appl. Cata. A: Gen. 500 (2015) 12–22.
[10] D. Liu, et al., MCM-41 supported nickel-based bimetallic catalysts with superior stability during carbon dioxide reforming of methane: effect of strong metal–support interaction, J. Catal. 266 (2) (2009) 380–390.
[11] G. Bonura, C. Cannilla, F. Frusteri, Ceria–gadolinia supported NiCu catalyst: a suitable system for dry reforming of biogas to feed a solid oxide fuel cell (SOFC), Appl. Catal. B: Environ. 121–122 (2012) 135–147.
[12] X. Fan, et al., Tuning the composition of metastable CoxNiyMg100-*x-y(OH)(OCH3) nanoplates for optimizing robust methane dry reforming catalyst*, J. Catal. 330 (2015) 106–119.
[13] I. Luisetto, S. Tuti, E. Di Bartolomeo, Co and Ni supported on CeO2 as selective bimetallic catalyst for dry reforming of methane, Int. J. Hydrogen Energy 37 (21) (2012) 15992–15999.
[14] M. Gong, et al., Sulfur-tolerant anode materials for solid oxide fuel cell application, J. Power Sources 168 (2) (2007) 289–298.
[15] Y. Matsuzaki, I. Yasuda, The poisoning effect of sulfur-containing impurity gas on a SOFC anode: part I. Dependence on temperature, time, and impurity concentration, Solid State Ionics 132 (3) (2000) 261–269.
[16] Z. Zhan, S.A. Barnett, An octane-fueled solid oxide fuel cell, Science 308 (5723) (2005) 844–847.
[17] A. Busawon, D. Sarantaridis, A. Atkinson, Ni infiltration as a possible solution to the redox Problem of SOFC anodes, Electrochem. Solid State Lett. 11 (10) (2008) B186–B189.
[18] M.D. Gross, J.M. Vohs, R.J. Gorte, Recent progress in SOFC anodes for direct utilization of hydrocarbons, J. Mater. Chem. 17 (30) (2007) 3071–3077.
[19] S. Park, R.J. Gorte, J.M. Vohs, Tape cast solid-oxide fuel cells for the direct oxidation of hydrocarbons, J. Electrochem. Soc. 148 (5) (2001) A443–A447.
[20] S. Park, J.M. Vohs, R.J. Gorte, Direct oxidation of hydrocarbons in a solid-oxide fuel cell, Nature 404 (6775) (2000) 265–267.
[21] T.Z. Sholklapper, et al., Nanostructured solid oxide fuel cell electrodes, Nano Lett. 7 (7) (2007) 2136–2141.
[22] T.Z. Sholklapper, et al., Synthesis and stability of a nanoparticle-infiltrated solid oxide fuel cell electrode, Electrochem. Solid State Lett. 10 (4) (2007) B74–B76.
[23] A. Atkinson, et al., Advanced anodes for high-temperature fuel cells, Nat. Mater. 3 (1) (2004) 17–27.
[24] Q. Fu, F. Tietz, D. Stöver, La0: 4Sr0 6Ti_{1-x} Mn_x $O_{3-\delta}$ perovskites as anode materials for solid oxide fuel cells, J. Electrochem. Soc. 153 (4) (2006) D74–D83.
[25] J.M. Haag, et al., Application of LaSr2Fe2CrO9-δ in solid oxide fuel cell anodes, Electrochem. Solid State Lett. 11 (4) (2008) B51–B53.
[26] S. McIntosh, R.J. Gorte, Direct hydrocarbon solid oxide fuel cells, Chem. Rev. 104 (10) (2004) 4845–4866.
[27] A. Ovalle, et al., Mn-substituted titanates as efficient anodes for direct methane SOFCs, Solid State Ionics 177 (19) (2006) 1997–2003.
[28] J. Peña-Martínez, et al., Anodic performance and intermediate temperature fuel cell testing of $La_{0.75}$: $Sr_{0.25}Cr_{0.5}Mn_{0.5}O_{3-\delta}$ at lanthanum gallate electrolytes, Chem. Mater. 18 (4) (2006) 1001–1006.
[29] S. Tao, J.T. Irvine, Catalytic properties of the perovskite oxide $La_{0.75}Sr_{0.25}Cr_{0.5}Fe_{0.5}O_{3-\delta}$ in relation to its potential as a solid oxide fuel cell anode material, Chem. Mater. 16 (21) (2004) 4116–4121.
[30] M. Feng, J. Goodenough, A superior oxide-ion electrolyte, Eur. J. Solid State Inorg. Chem. 31 (8–9) (1994) 663–672.
[31] T. Ishihara, H. Matsuda, Y. Takita, Doped LaGaO3 perovskite type oxide as a new oxide ionic conductor, J. Amer. Chem. Soc. 116 (9) (1994) 3801–3803.
[32] X. Zhang, et al., Interface reactions in the NiO–SDC–LSGM system, Solid State Ionics 133 (3) (2000) 153–160.
[33] X. Liu, et al., Impregnated nickel anodes for reduced-temperature solid oxide fuel cells based on thin electrolytes of doped LaGaO 3, J. Power Sources 222 (2013) 92–96.
[34] Z. Zhan, et al., A reduced temperature solid oxide fuel cell with nanostructured anodes, Energy Environ. Sci. 4 (10) (2011) 3951–3954.
[35] Z. Salehi, et al., Porous/dense $La_{0.8}Sr_{0.2}Ga_{0.8}Mg_{0.2}O_{3-\delta}$ (LSGM) bilayer infiltrated with metallic oxidation catalyst, Ceram. Int. 40 (10) (2014) 16455–16463.
[36] Z. Salehi, et al., Spin-Coated $La_{0.8}$: $Sr_{0.2}Ga_{0.8}Mg_{0.2}O_{3-\delta}$ electrolyte on infiltrated anodes for direct methane fuel cells, ECS Trans. 57 (1) (2013) 1371–1378.
[37] J. Wei, E. Iglesia, Isotopic and kinetic assessment of the mechanism of reactions of CH4 with CO2 or H2O to form synthesis gas and carbon on nickel catalysts, J. Catal. 224 (2) (2004) 370–383.
[38] B. Bachiller-Baeza, et al., Transient studies of low-temperature dry reforming of methane over Ni-CaO/ZrO2-La2O3, Appl. Catal. B: Environ. 129 (2013) 450–459.
[39] K. Takanabe, et al., Titania-supported cobalt and nickel bimetallic catalysts for carbon dioxide reforming of methane, J. Catal. 232 (2) (2005) 268–275.
[40] W. An, et al., Catalytic activity of bimetallic nickel alloys for solid-oxide fuel cell anode reactions from density-functional theory, J. Power Sources 196 (10) (2011) 4724–4728.
[41] J. Zhang, H. Wang, A. Dalai, Development of stable bimetallic catalysts for carbon dioxide reforming of methane, J. Catal. 249 (2) (2007) 300–310.
[42] K. Nagaoka, Modification of Co/TiO2 for dry reforming of methane at 2 MPa by Pt, Ru or Ni, Appl. Cata. A: Gen. 268 (1–2) (2004) 151–158.